

Preparation and characterization of inexpensive submicron range inorganic microfiltration membranes

B.K. Nandi, B. Das, R. Uppaluri* and M.K. Purkait

Department of Chemical Engineering, Indian Institute of Technology Guwahati
Guwahati - 781039, Assam, India

(Received December 1, 2009, Accepted February 9, 2010)

Abstract. This work presents inexpensive inorganic precursor formulations to yield submicron range symmetric ceramic microfiltration (MF) membranes whose average pore sizes were between 0.1 and 0.4 μm . Incidentally, the sintering temperature used in this work was about 800 to 950°C instead of higher sintering temperatures (1100°C) that are usually deployed for membrane fabrication. Thermogravimetric (TGA) and X-Ray diffraction (XRD) analysis were carried out to evaluate the effect of temperature on various phase transformations during sintering process. The effect of sintering temperature on structural integrity of the membrane as well as pore size distribution and average pore size were evaluated using scanning electron microscopy (SEM) analysis. The average pore sizes of the membranes were increased from 0.185 to 0.332 μm with an increase in sintering temperature from 800 to 950°C. However, a subsequent reduction in membrane porosity (from 34.4 to 19.6%) was observed for these membranes. Permeation experiments with both water and air were carried out to evaluate various membrane morphological parameters such as hydraulic pore diameter, hydraulic permeability, air permeance and effective porosity. Later, the membrane prepared with a sintering temperature of 950°C was tested for the treatment of synthetic oily waste water to verify its real time applicability. The membrane exhibited 98.8% oil rejection efficiency and $5.36 \times 10^{-6} \text{ m}^3/\text{m}^2 \cdot \text{s}$ permeate flux after 60 minutes of experimental run at 68.95 kPa trans-membrane pressure and 250 mg/L oil concentration. Based on retail and bulk prices of the inorganic precursors, the membrane cost was estimated to be \$220 / m^2 and \$1.53 / m^2 , respectively.

Keywords: ceramic membrane; submicron; kaolin; oil-in-water; sintering.

1. Introduction

Existing and ongoing policies in process industries enforce the replacement of conventional process technology with membrane technology. Some of the aspiring features that membrane technology bestows include compact design, high product quality and lower operating cost. Alumina (DeFriend, *et al.* 2003, Gestel, *et al.* 2002), zirconia (Falamaki, *et al.* 2004), titania (Wang, *et al.* 2006) and silica (Yoshino, *et al.* 2005) based ceramic membranes with high chemical, mechanical and thermal stability and longer life time are found to be useful in different membrane based applications. However, the cost of these membranes is very high compared to polymeric membranes. This is primarily due to the higher cost of the inorganic precursors (alumina, zirconia, titania, silica) as well as very high sintering temperature (more than 1100°C) required for the fabrication of membrane. This is also due to the fact that higher sintering temperatures demand higher electrical energy and hence operating costs. In addition, higher sintering temperatures may also give rise to enhancement

* Corresponding author, Ph.D. E-mail: ramgopalu@iitg.ernet.in

in furnace power specifications and installed cost. Due to these key issues, the economic competitiveness of the inorganic membranes has not been appreciable till date to drive their industrial sustainability. To circumvent the higher costs of inorganic membranes, existing and ongoing research in the preparation of low cost inorganic membranes is dovetailed towards the usage of low cost inorganic precursors and lower sintering temperatures (below 1000°C). However, these variants in ceramic membrane research need to guarantee cheaper membranes that have the inherent ability to provide consistent performance along with longer life time, in similarity to the existing expensive ceramic membranes.

Recently, much work has been reported for the fabrication of inorganic membranes using cheaper raw materials such as apatite powder (Masmoudia, *et al.* 2007), fly ash (Saffaj, *et al.* 2004), natural raw clay (Saffaj, *et al.* 2006, Khemakhem, *et al.* 2009), dolomite (Bouzerara, *et al.* 2006), kaolin (Belouatek, *et al.* 2005, Chen, *et al.* 2008, Workneh and Shukla 2008, Nandi, *et al.* 2008). Table 1 summarizes the details of raw materials, average pore size and sintering temperature used in these works. From the table it can be observed that for all the cases, the sintering temperature used was more than 1100°C and the average pore size of the membranes was more than 1 µm (except alumina and zirconia). Our recent work (Nandi, *et al.* 2008) reported the fabrication of low cost ceramic membranes whose average membrane pore size was within the moderately upper micron range (0.7 to 1.54 µm). For these membranes, the sintering temperature was lower than 1000°C. Also, it is well known that microfiltration (MF) membranes with pore size in the submicron range (0.1 to 0.4 µm) are preferred for the industrial application to obtain excellent solute separation efficiency. With regards to the submicron range ceramic filters available so far, it is also equally important to note that these ceramic membranes consist of an asymmetric membrane structure. These asymmetric membranes typically consist of a submicron skin layer prepared using zeolite (Workneh and Shukla 2008, Potdar, *et al.* 2002), zirconia, alumina (Saffaj, *et al.* 2006), and titania (Das and Dutta 1999) on either single or several layers of macroporous structures. Though such an approach favors the reduction of the overall cost of the membrane by limiting the thickness of the skin layer (expensive), the utilization of expensive precursors such as zeolite and alumina to fabricate the skin layer contributes to the overall cost of the membrane. In addition, preparation methods for asymmetric membranes in contrast to

Table 1 Summary of literatures on submicron range homogeneous microfiltration membrane

Materials	Sintering temperature (°C)	Average pore diameter (µm)	Reference
α-Alumina	1130-1300	0.1-0.2	Gestel, <i>et al.</i> 2002
α-Alumina	1300-1500	0.17-0.15	Falamaki, <i>et al.</i> 2004
Zirconia	1300-1500	0.11 -0.08	Falamaki, <i>et al.</i> 2004
Apatite powder	1150-1200	5-8	Masmoudia, <i>et al.</i> 2007
Fly ash	1100-1130	4-4.9	Jedidi, <i>et al.</i> 2009
Cordierite	1275	7	Saffaj, <i>et al.</i> 2004
Natural clay	1100-1250	9.3-10.75	Saffaj, <i>et al.</i> 2006
Natural clay	1190	9.2	Khemakhem, <i>et al.</i> 2009
Dolomite and kaolin	1150-1300	1.65-48.53	Bouzerara, <i>et al.</i> 2006
Kaolin and hycast clay	1100	1.3	Belouatek, <i>et al.</i> 2005
Kaolin and Al(OH) ₃	1500-1550	1.16-1.52	Chen, <i>et al.</i> 2008
Kaolin, CaCO ₃ , quartz	850-1000	0.7-1.54	Nandi, <i>et al.</i> 2008
Kaolin, feldspar, quartz	800-950	0.185-0.332	Present work

the symmetric membranes involve additional fabrication complexities that also contribute to the overall cost. Therefore, it is apparent that the fabrication of a symmetric ceramic MF membrane possessing sub-micron range average pore size (0.1-0.4 μm) using low cost inorganic precursors and sintering temperature lower than 1000°C has not been addressed so far.

In continuation to our previous efforts (Nandi, *et al.* 2008), the objective of this work was to identify suitable low cost inorganic precursor formulation that can yield an inexpensive stable ceramic membrane with nominal pore sizes below 0.4 μm using a sintering temperature below 1000°C. Different low cost inorganic raw materials such as kaolin, quartz, feldspar, sodium carbonate, boric acid and sodium metasilicate were used for the preparation of the ceramic membrane. Thermal, structural and morphological studies of the prepared membranes were carried out to evaluate the general characteristics of the fabricated ceramic membrane. Both liquid and gas permeation experiments were performed to evaluate different membrane parameters such as hydraulic permeability, hydraulic pore diameter, porosity of the membranes along with percent macropores and mesopores present in the porous membrane structure. Further, the applicability of the prepared inexpensive inorganic membrane for industrial purpose was verified by the separation of oil-in-water (o/w) emulsions. Finally, the cost analysis of the prepared membranes based on retail as well as bulk material cost were also carried out to compare the cost of membrane with other similar membranes available in market.

2. Experimental

2.1. Raw materials

This work utilized six common inorganic raw materials such as kaolin (CDH, India), quartz (Research Lab Fine Chem Industry, India), feldspar (National Chemicals Ltd, India), sodium carbonate (Merck India), boric acid (Merck India) and sodium metasilicate (SD Fine Chem Ltd, India). All these raw materials used for inorganic fabrication were graded atleast 99.5% pure and were used without any further purification. Different raw materials used in this work for the fabrication of inorganic membrane served for different functional attributes. Kaolin and feldspar provided low plasticity and high refractory properties to the membrane. Quartz contributed to the mechanical and thermal stability of the membrane. Regulation of porous texture in the ceramic was realized by sodium carbonate which under sintering conditions dissociated into Na_2O and released CO_2 gas. The path taken by the released CO_2 gas thereby created the porous texture of the inorganic membrane and contributed to the membrane porosity during the sintering process. Boric acid increased membrane mechanical strength by the formation of metallic metaborates at sintering temperatures. Boric acid and sodium carbonate also act as colloidal agents and improved dispersion properties of the inorganic precursors thereby addressing homogeneity in the membrane structure. In a similar way, sodium metasilicate acts as a binder by creating silicate bonds among the elements to induce higher mechanical strength in the ceramic membrane. The final formulation reported in this work has been deduced from a trial and error based fabrication approach using various ratios of inorganic precursors. The suggested precursor formulation provides a crack free membrane with good structural integrity and desired submicron range pore diameters.

Three major clay materials i.e., kaolin, feldspar and quartz used for the membrane fabrication process were characterized using X-Ray diffraction analysis (Make: Bruker Axs; Model: D8 ADVANCE, USA) and particle size distribution analysis (Make: Malvern; Model: Mastersizer 2000, UK). The

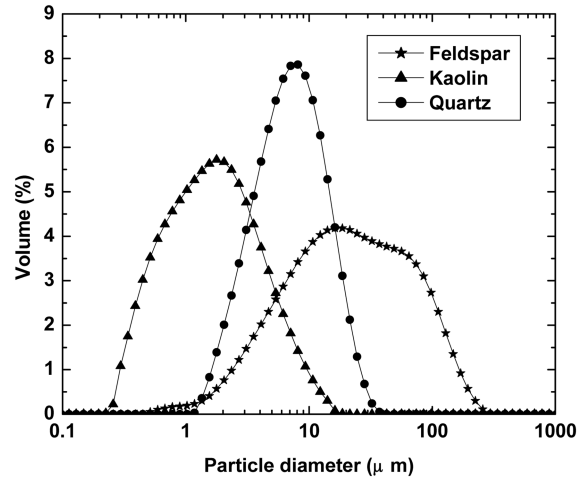


Fig. 1 Particle size distribution for different raw materials

XRD spectrum of the clay materials were matched with the JCPDS (Joint Committee on Powder Diffraction Standards) (JCPDS 1997) database file PDF-01-089-6538, PDF-01-075-0443 and PDF-01-089-8574 for kaolin, quartz and feldspar, respectively. Results obtained from particle size analysis of clay materials are shown in Fig. 1. From the figure, it can be observed that particle size of the kaolin varied from 18.67 to 0.224 μm , 240 to 0.479 μm for feldspar and 37.24 to 1.18 μm for quartz. The average particle size of kaolin, feldspar and quartz were 2.37, 36.32 and 8.4 μm , respectively.

2.2. Membrane fabrication

The inorganic precursor formulation to yield a sub-micron range ceramic membrane was identified based on a trial and error procedure. The ceramic MF membrane was prepared from a clay mixture with a specific composition (as presented in Table 2) using a laboratory blender (Model: Laboratory Blender; Make: Remi Anupam Mixie Ltd, Mumbai, India) followed by addition of distilled water to

Table 2 Composition and cost analysis of fabricated membrane from unit retail and bulk price of raw materials

Material	Composition wet basis (wt %)	Composition dry basis (wt %)	Retail unit price (\$/kg)	Bulk unit price	
				(\$/kg)	Reference
Kaolin	37.04	50	5	0.12	ICIS, 2009
Quartz	11.11	15	64	0.084	China Glass Network, 2009
Feldspar	11.11	15	70	0.083	U.S. Geological Survey, 2006
Sodium carbonate	7.41	10	4.6	0.185	ICIS, 2009
Boric acid	3.7	5	5.6	0.836	ICIS, 2009
Sodium metasilicate	3.7	5	8.4	0.4	Sichuan, 2009
Water	25.93	0	0	0	

Total numbers of membranes prepared per kg dry mixture = 50

(0.02 kg dry mixture/membrane of 4.5 mm thickness and 52.5 mm diameter)

Total surface area obtained = $50 \times 3.14 \times (0.0525)^2 / 4 = 0.108 \text{ m}^2$

Cost of the membranes = 220 $\$/\text{m}^2$ 1.53 $\$/\text{m}^2$

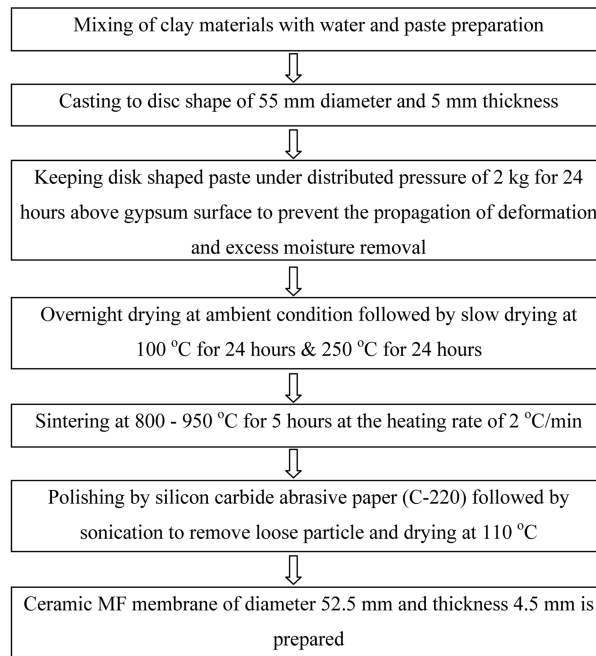


Fig. 2 Block diagram for the preparation of ceramic membrane from raw materials

prepare a paste. A summary of the preparation method are shown in Fig. 2. The fabrication methodology was consistently maintained as a simple process and is similar to the procedure reported previously. Four different sintering temperatures 800, 850, 900 and 950°C were used to prepare ceramic membrane with different morphology in order to evaluate the effect of sintering temperature on the structure and morphology of the membranes.

2.3. Experimental set up

A schematic of experimental set up used for both air and water permeation experiment is presented in Fig. 3. The set up constitutes a Teflon tubular cell (125 ml capacity) with a flat circular teflon base plate that houses the ceramic membrane. Membranes were kept in the teflon casing and sealed with epoxy resin (Mseal, Pidilite Industries Ltd, Mumbai, India). During air permeation experiments, the outlet of the setup was connected to a gas flow meter using a silicon tube for measuring the gas flow rate at various trans-membrane pressure differentials. For pure water flux and o/w emulsions, the feed (de-ionized water and o/w emulsions) was filled in the tubular section from the top. The cell was pressurized with compressed air. Liquid permeate flux was measured using a digital scale weight machine.

2.4. Characterization techniques

Thermogravimetric analysis (TGA) and differential thermal analysis (DTA) (Make: Mettler Toledo; Model: TGA/SDTA 851^e, USA) of the sample mixture was carried out to identify the various thermal transformations of the material during sintering. X-Ray diffraction analysis (XRD) analysis of the

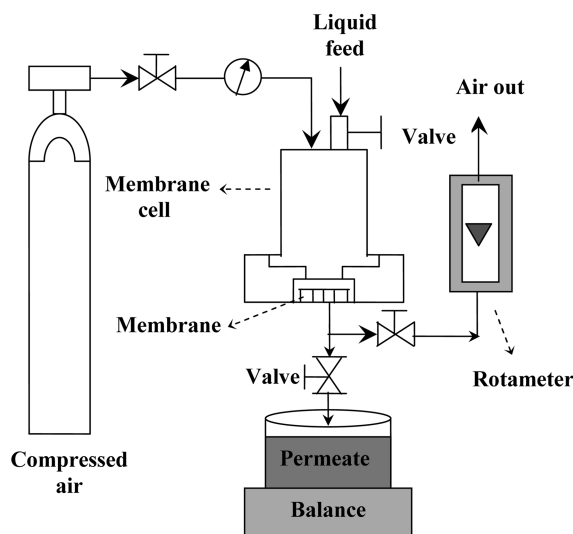


Fig. 3 Experimental setup for the permeation experiments

inorganic membrane was conducted to evaluate the extent of phase transformations. Scanning electron microscopic (SEM) study (Make: Oxford; Model: LEO 1430VP, UK) was carried out to analyze the presence of possible defects and estimate the membrane pore size. The estimation of average membrane pore size (d_s) from SEM micrographs was carried out using ImageJ software (Version 1.40) (Nandi, *et al.* 2008, Chakrabarty, *et al.* 2008a). The open porosity of the membrane was evaluated using Archimedes method with water as the wetting liquid. Air permeation experiments were conducted to quantify membrane morphological parameters such as average pore size (d_g) and effective porosity that contribute to the transport. Permeation experiments using pure water (deionised water) were conducted for the estimation of hydraulic permeability (P_m) and hydraulic pore diameter (d_l) of the membrane. Before conducting liquid permeation experiments, the membranes were compacted at a trans-membrane pressure of 414 kPa (higher than the maximum operating pressure for the set of experiments i.e. 345 kPa). During these experiments, the pure water flux (PWF) was observed to be high initially and reduced to the steady value after two hours of operation for all the membranes. For the membrane sintered at 900°C, the observed pure water flux at the beginning of compaction was $6.4 \times 10^{-4} \text{ m}^3/\text{m}^2.\text{s}$ which subsequently reached to a steady state value of $5.0 \times 10^{-4} \text{ m}^3/\text{m}^2.\text{s}$.

2.5. Microfiltration of oil-in-water emulsions

Microfiltration (MF) experiments of synthetic o/w emulsions were carried out to verify the applicability of the membrane for real time applications. Crude oil was collected from Guwahati Refinery, Indian Oil Corporation Limited (IOCL), India. The emulsions were prepared by placing the o/w mixture in a sonicator tank (Make: Elmasonic; Model: S30H) for 15 hours at a temperature of 25°C. MF experiments were carried out with two different concentrations of crude oil (125 and 250 mg/L) and four trans-membrane pressure differential (ΔP) (68.95, 137.90, 206.84 and 275.79 kPa) to observe the effect of oil concentration and ΔP on the permeate flux and oil rejection efficiency. All the experiments were conducted at room temperature (~25°C). The permeate flux (J) and the percent oil rejection (R) were calculated using the following equations:

$$J = \frac{V}{S \times \Delta t} \quad (1)$$

$$R = \left(1 - \frac{C_p}{C_f}\right) \times 100 \quad (2)$$

where, J ($\text{m}^3/\text{m}^2.\text{s}$) is the permeate flux through the membrane, V (m^3) is the volume of permeate, S (m^2) is the effective membrane area, Δt (s) is the sampling time, R is the percent oil rejection efficiency, C_f and C_p (mg/L) are the concentration of oil in the feed and permeate, respectively. C_f and C_p were determined using a UV-Vis spectrophotometer (Make: Perkin Elmer Precisel; Model: Lambda 35, USA) by measuring absorbance at a wave length of 235 nm where maximum absorbance was observed (Chakrabarty, *et al.* 2008b).

3. Results and discussion

3.1. Structural characterization

3.1.1. Thermogravimetric analysis

The objective of thermal analysis was to identify temperature regimes where predominant weight losses (and hence transformations) occur in the membrane matrix. Thereby, an insight can be obtained for analyzing the effect of various temperature regimes on the porous structure, pore diameter and mechanical strength of the membrane. Fig. 4 presents the results obtained from TGA and DTA of the powder mixture when the dry inorganic mixture was heated in a α -alumina crucible from room temperature to 1000°C at a heating rate of 10°C per minute. The figure conveys that a highly non-linear variation exists due to the presence of complex phase transformations and interactions. The total weight loss of the sample was observed to 19.5%. About 5% weight loss was observed below 106°C due to the removal of weakly bonded water molecules in the sample mixture. This specific water loss was characterized by an endothermic peak at 106°C in the DTA curve. The

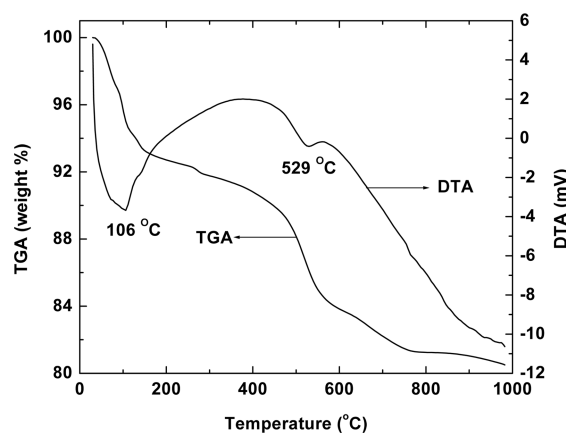


Fig. 4 TGA-DTA curves

weight loss of the sample between temperatures of 106 to 400°C was around 4.5%, which were correlated with the pre-dehydration process of kaolin and dehydration of crystal water of boric acid. The pre-dehydration process of kaolin occurs due to the reorganization of the octahedral layer (Balek and Murat 1996). The second endothermic peak in the DTA curve was corresponding to the total weight loss of 5% in between temperatures of 400 to 540°C. This was due to the transformation of kaolinite to metakaolinite that involves the loss of structural hydroxyl groups at 529°C according to the following reaction:



The formation of CO₂ (and hence enhancement of the porous structure of the membrane) occurred at 730°C and corresponds to a weight loss of 2% in the temperature regime of 663°C to 764°C due to calcinations of Na₂CO₃ in this temperature regime. The sample corresponded to very insignificant weight loss above 764°C as conveyed by the TGA curve. This observation further justifies that all phase transformations are complete below the chosen sintering temperature range (800-950°C) in this work, a value that is well below the usual sintering temperature 1100°C presented in various works (Masmoudia, *et al.* 2007, Saffaj, *et al.* 2004, 2006, Bouzerara, *et al.* 2006, Belouatek, *et al.* 2005, Chen, *et al.* 2008).

3.1.2. X-Ray diffraction analysis

From the TGA- DTA analysis it was observed that above sintering temperature of 764°C almost no significant weight loss was occurred. To verify this observation XRD analysis of membrane structure at temperature higher than 764°C was carried out. Fig. 5 summarizes XRD graphs for four different samples calcined at 25, 800, 900 and 950°C for five hours in muffle furnace. The observation of peaks and trends in the XRD graphs convey that the inorganic mixture originally consisted of

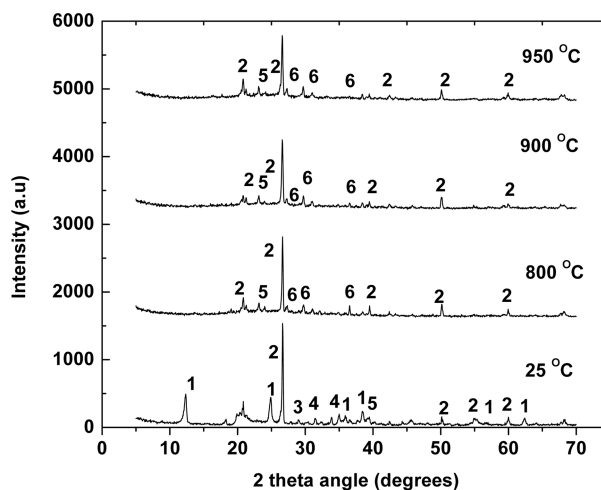


Fig. 5 X-ray diffraction patterns of the sample mixture sintered at different temperature. 1; Kaolinite (PDF-01-089-6538), 2; Quartz (PDF-01-075-0443), 3; Hydrogen Borate (PDF-00-022-1109), 4; Sodium Calcium Silicate (PDF-00-002-0951), 5; Inyoite (PDF-00-006-0361), 6; Nephiline (PDF-00-019-1176)

kaolinite, quartz, hydrogen borate, sodium calcium silicate and inyoite as main components. The XRD graph obtained for the sample calcined at 800°C (Fig. 4) depicts that peaks corresponding to kaolinite have disappeared due to conversion of kaolinite to metakaolinite. In this regard, the TGA - DTA curve (Fig. 4) indicates the phase formation of metakaolinite at 529°C, due to which kaolinite peak disappeared in the XRD graph for the sample calcined at 800°C. The other phases that appear are nephiline and quartz. Nephiline (Na_2O , Al_2O_3 , 2SiO_2) is produced by the reaction of sodium oxide (Na_2O) and metakaolinite at temperature around 800°C (Wang, *et al.* 1994). A critical observation of the peaks at higher temperature reveals that no other significant phase transformation occurs above 800°C to 950°C. This signifies that the membrane skeletal structure constitutes mainly metakaolinite, quartz and nephiline. From the XRD analysis it may also be concluded that the sintering temperature of 800°C was sufficient for the preparation of membranes. All XRD diffractogram graphs indicate no change in the peak trends corresponding to quartz thereby inferring that quartz phase was not at all affected by sintering of inorganic materials within the studied temperature range considered in this work. Therefore the sintering temperature between 800 to 950°C for inorganic membrane synthesis can be inferred to be appropriate.

3.1.3. Surface morphology

Fig. 6 illustrates SEM pictures for the membrane sintered at four different temperatures considered

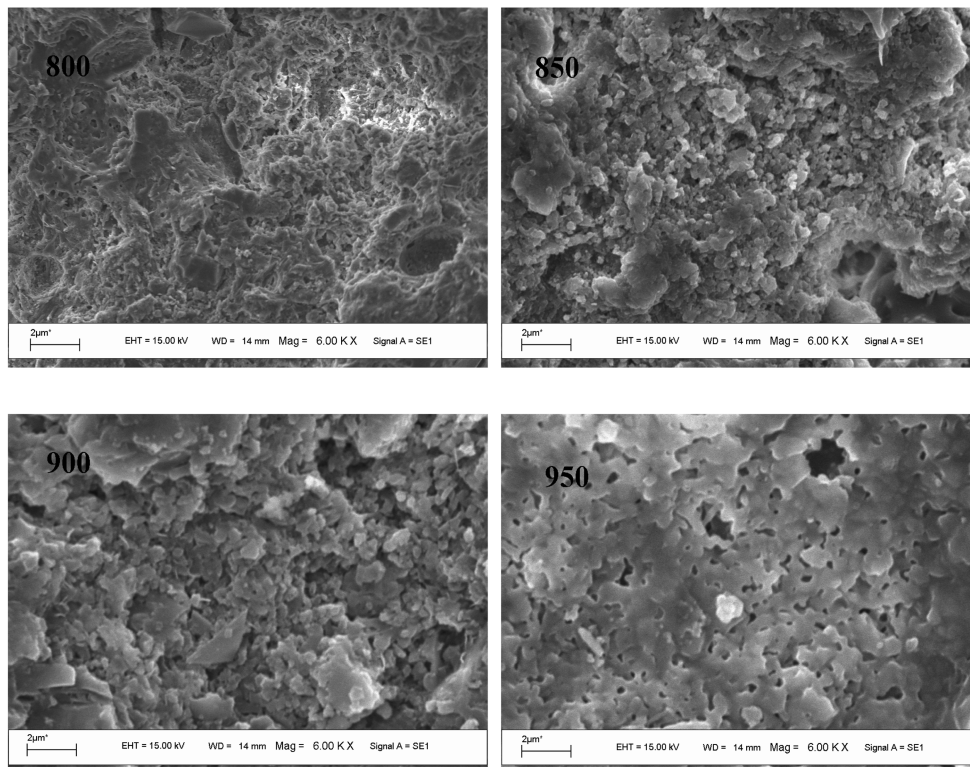


Fig. 6 SEM photographs of the prepared microfiltration membranes surface sintered at 800°C, 850°C, 900°C and 950°C

Table 3 Average pore diameter and pore size ranges obtained from SEM analysis

Sintering temperature (°C)	Pore diameter (d_s , μm)	% pores with pore diameters between 0.1-0.3 μm
800	0.185	90.07
850	0.239	87.14
900	0.285	82.67
950	0.332	75.14

in this work. All membranes were observed to possess surface with a rough morphological structure. Membranes sintered at lower temperature (800 and 850°C) possess highly porous structure. The membrane sintered at 900 and 950°C were more consolidated due to the fact that for sintering temperatures over 850°C, the particles agglomerate together creating more dense ceramic structure. As a result the porosity of the membrane decreased with increase in sintering temperature. A superficial observation of the SEM indicated that the membrane did not have any pinholes cracks and the maximum observable pore size of the surface was about 2 μm . These attributes of the membrane make it suitable for MF applications. The area average pore diameter (d_s) of the membrane was estimated using standard method (Nandi, *et al.* 2008). To do so, five different SEM images were taken randomly from different locations of the membrane and were evaluated for pore size distributions using ImageJ software (Version 1.40). The average pore diameters of membranes were evaluated to be 0.185, 0.239, 0.285 and 0.332 μm for membranes sintered at 800, 850, 900 and 950°C, respectively (Table 3). The average pore size of the membranes was closely related to the sintering temperature. For all sintering temperatures, maximum numbers of pores (75 to 90%) were in the range of 0.1 to 0.3 μm . The mean pore size of the membranes increased with an increase in the sintering temperature, and the pore size distribution broadened at the same time. This was due to the growth of grains at higher sintering temperatures that lead to the formation of larger pores and elimination of smaller pores.

3.1.4. Porosity and structural density

Total porosity of the membrane were estimated using Archimedes principle by measuring the

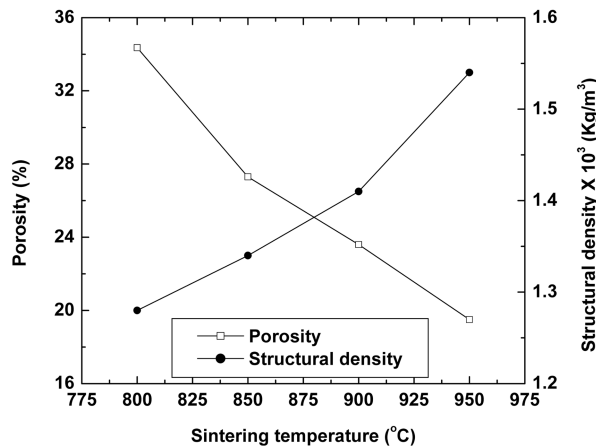


Fig. 7 Porosity and structural density of membranes sintered at various temperatures

volume of the wetting liquid that displaced air in a dry membrane after equilibrating the membrane with water for 12 hours. Fig. 7 shows the variation of membrane porosity and structural density of membranes with varying sintering temperature. From the figure, it can be observed that structural density of the membrane increased and total porosity decreased with an increase in sintering temperature. The membrane porosity and structural density of the membrane sintered at 800°C were 34.4% and 1280 kg/m³, respectively. When the sintering temperature was increased to 950°C, porosity of the membrane decreased to 19.5% and the structural density increased to 1540 kg/m³. This was due to the fact that with increase in sintering temperature densification of the porous structure occurs and thereby allows for an increase in structural density and decrease in the membrane porosity. This is also reasoned with the fact that with increasing sintering temperature, the number of pores representing small pore sizes has reduced and hence the overall pore volume and porosity decreased.

3.2. Permeation characteristics

3.2.1. Gas transport characteristics

The average pore diameter and effective porosity of the membrane were also evaluated from the gas (air) permeation experiments. The distribution of percentage pores in the macropores (pore dia >50 nm) and mesopores (pore dia <50 nm) (Mulder 1991) in the membrane matrix can be conveniently determined using this experiments (Nandi, *et al.* 2009). Average pore diameter (d_g) and effective porosity (ε/q^2) of the membrane were determined from the plot of effective permeability factor (K) of the membrane and average pressure on the membrane (P) using following expressions as

$$K = 2.133 \times \frac{r \times v_g}{l} \times \frac{\varepsilon}{q^2} + 1.6 \times \frac{r^2}{l \times \eta} \times \frac{\varepsilon}{q^2} \times P \quad (3)$$

$$d_g = 2 \times r = 2.666 \times \frac{B}{A} \times v_g \times \eta \quad (4)$$

where,

$$A = 2.133 \times \frac{r \times v_g}{l} \times \frac{\varepsilon}{q^2} \quad (5)$$

$$B = 1.6 \times \frac{r^2}{l \times \eta} \times \frac{\varepsilon}{q^2} \quad (6)$$

and

$$K = \frac{Q \times P_2}{S \times \Delta P} \quad (7)$$

where, l (m) is the length of the pore, v_g (m/s) is the molecular mean velocity of the gas, η (kPa.s) is the viscosity of gas, r (m) is the pore radius of the membrane, P_2 (kPa) membrane pressure at permeate side. d_g were calculated using Eq. (4) for known values of η , v , A and B , A and B were obtained from the linear plot of K vs. P as intercept (A) and slope (B). After calculating the values of d_g , effective porosity of the membrane was calculated using Eq. (5) for known values of A . In Eq. (3), the first term (intercept) corresponds to Knudsen permeance and the second term (slope) corresponds to the viscous permeance. Henceforth, the values of the slope and intercept obtained

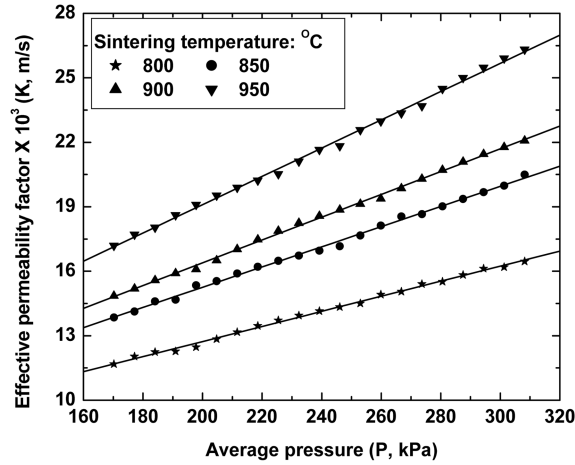


Fig. 8 Variation of effective permeability factor with average pressure for the different membranes

Table 4 Various parameters evaluated from graphical analysis of air permeation flux data

Sintering temperature (°C)	Intercept (A)×10 ³ (m/s)	Slope (B)×10 ⁸ (m/s.Pa)	Pore diameter (d_g , μm)	Effective porosity ($\frac{\epsilon}{q^2}$)	Contribution of viscous flux (%)	Contribution of Knudsen flux (%)
800	5.72	3.50	0.157	0.386	53-67	47-33
850	5.79	4.70	0.197	0.326	59-73	41-27
900	5.87	5.30	0.218	0.276	63-75	37-25
950	5.94	6.68	0.279	0.241	67-79	33-21

from the graph were also used to evaluate the percentage contribution of pores (and pore sizes) that contributed towards viscous and Knudsen flow transport through the membrane.

Fig. 8 presents the variation of effective permeability factor (K) with average pressure (P) varying from 170 to 308 kPa for different membranes. The measured gas permeance of different membranes were 1.26×10^{-4} , 1.544×10^{-4} , 1.63×10^{-4} and 1.93×10^{-4} m³/m².s.kPa at trans-membrane pressure drop of 206.84 kPa for sintering temperature of 800, 850, 900 and 950°C, respectively. Table 4 summarizes parameters evaluated from the graphical analysis of permeate flux data obtained from air permeation experiments. As shown in the table, the average pore diameter of the membrane obtained from theoretical analysis of permeation experiments varied from 0.157 to 0.279 μm. In this regard, measured pore diameter from SEM analysis (as reported in section 3.1.3) varied from 0.185 μm to 0.332 μm. The table also summarizes effective porosity factor values ranging from 0.386 to 0.241 that truly represents and contributes to the membrane transport. In this regard, it can be observed that the total porosity of the membrane varied from 0.344 to 0.195 (section 3.1.4) which is close to the predicted value of the effective porosity. Therefore, the assumption of cylindrical pores in the calculation procedure was justified with the fact that tortuosity was close to one.

Table 4 infers that for membrane sintered at 900°C, viscous flux contributes 63 to 75 percent to the total flux conveying that about 63 to 75 percent of the pores in the membrane have pore sizes well above the regime where Knudsen diffusion dominates the transport (1 to 20 nm). A similar

observation can be made from the permeation analysis of other membranes where it is found that viscous flux contributes 53 to 67 percent, 59 to 73 percent and 67 to 79 percent of the total flux for 800, 850 and 950°C membranes, respectively. The Knudsen flow regime and hence pores in the range of 1 to 20 nm represents 33 to 47 percent, 27 to 41 percent, 25 to 37 percent and 21 to 33 percent of the pore size contributing to the transport mechanism for membrane sintered at 800, 850, 900 and 950°C, respectively. The reduction in the percent contribution of Knudsen flux to the total flux with increasing sintering temperatures is due to enhancement in the consolidation of membrane structure at higher sintering temperatures as outlined in section 3.1.3 and Fig. 6.

3.2.2. Hydraulic pore diameter, permeability and effective permeable area factor

The hydraulic permeability (P_m) and hydraulic pore radius (d_l) of the membranes were evaluated by assuming presence of cylindrical pores in the membrane matrix using the following expression (Mulder 1991)

$$J_w = \frac{\Delta P \varepsilon_m d_l^2}{\mu_w 32 l_m} = P_m \times \Delta P \quad (8)$$

$$P_m = \frac{\varepsilon_m d_l^2}{32 \times l_m \times \mu_w} \quad (9)$$

$$d_l = \left[\frac{32 \times \mu_w \times l_m \times P_m}{\varepsilon_m} \right]^{0.5} \quad (10)$$

In Eq. (9), $\varepsilon_m d_l^2$ correspond to effective permeable area factor that determines the actual permeable area available during filtration. It can also be analyzed that higher values of $\varepsilon_m d_l^2$ enable higher permeate fluxes and hence higher permeability of the membrane.

Table 5 presents the variation of hydraulic pore diameter and hydraulic permeability of the membranes with sintering temperatures. As shown, the hydraulic pore diameter of the membrane increased from 0.237 to 0.645 μm by increasing the sintering temperature from 800 to 950°C and hence $\varepsilon_m d_l^2$ (from 19.32×10^{-3} to $81.12 \times 10^{-3} \mu\text{m}^2$) as well as P_m (1.51×10^{-10} to $6.33 \times 10^{-10} \text{ m}^3/\text{m}^2 \cdot \text{s} \cdot \text{Pa}$) also increased. Enhancement in hydraulic pore diameter with an increase in sintering temperature was due to the growth of grains at higher sintering temperatures that lead to the formation of larger pores and elimination of smaller pores from the porous structure (as discussed in section 3.1.3). Similar trends were reported in literature for other clay based inorganic membranes (Saffaj, *et al.*

Table 5 Characteristic parameters obtained from water permeation experiments for membranes fabricated at various sintering temperatures

Sintering temperature (°C)	Hydraulic pore diameter (d_l , μm)	Total porosity (ε_m)	Effective permeable area factor ($\varepsilon_m d_l^2 \times 10^3$, μm^2)	Permeability ($P_m \times 10^{10}$, $\text{m}^3/\text{m}^2 \cdot \text{s} \cdot \text{Pa}$)
800	0.237	0.344	19.32	1.51
850	0.359	0.273	35.18	2.75
900	0.511	0.236	61.62	4.83
950	0.645	0.195	81.12	6.33

2006) as well as polymeric membranes (Chakrabarty, *et al.* 2008a).

With respect to the observable trends of average pore diameter calculated from SEM (d_s presented in Table 3), air permeation (d_g presented in Table 4) and pure water permeation (d_l presented in Table 5), it was observed that the average pore diameter calculated from air permeation experiment was smaller than the values calculated from SEM analysis. This was due to the fact that in SEM analysis using ImageJ software, comparatively pores greater than 50 nm were considered on the membrane surface. So, there was a possibility that this method may overestimate the mean pore size by considering the wider pores on the surface and overlooking the smaller pores. Average pore diameter calculated from air permeation (d_g) gives the minimum pore diameter and pure water permeation (d_l) gives the highest pore diameter. This is because of the fact that gas molecules are more likely to pass through small voids or interstices than water molecules.

3.3. Microfiltration of oil-in-water emulsions

The membrane sintered at 950°C was used for the MF of o/w emulsions. Figs. 9 and 10 illustrate the time dependent permeate flux profiles for 125 and 250 mg/L crude oil feed concentration, respectively, at various ΔP ranging from 68.95 to 275.79 kPa. From both the figures, it was observed that the permeate flux declined sharply within the initial 10 to 15 minutes of operation and becomes gradual thereafter. The permeate flux decreased from 32.6×10^{-6} to 5.4×10^{-6} m³/m².s at the end of 60 minutes of experimental run at a trans-membrane pressure drop of 68.95 kPa (Fig. 9). This decline in flux with time was due to pore blocking of ceramic porous structure and concentration polarization over the membrane surface. It is also observed that permeate flux increases with increase in trans-membrane pressure. From Fig. 9 it may be observed that at permeate flux increased from 32.6×10^{-6} to 62.2×10^{-6} m³/m².s when ΔP was increased from 68.95 to 275.79 kPa. An increase in permeate flux with ΔP was due to the higher driving force across the membrane. Similar flux decline trends with trans-membrane pressure and operating time were also observed for 250 mg/L oil concentrations as shown in Fig. 10. From both the figures, it may be found that

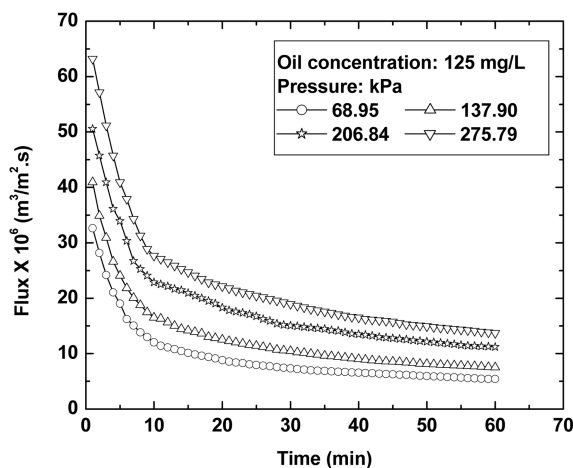


Fig. 9 Variation of permeate flux with time at different trans-membrane pressure. Initial oil concentration: 125 mg/L

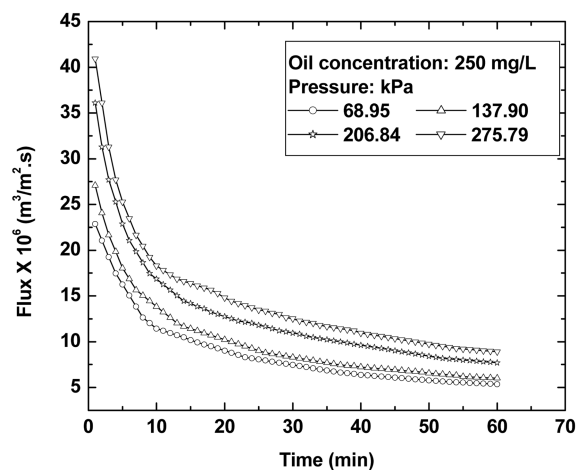


Fig. 10 Variation of permeate flux with time at different trans-membrane pressure. Initial oil concentration: 250 mg/L

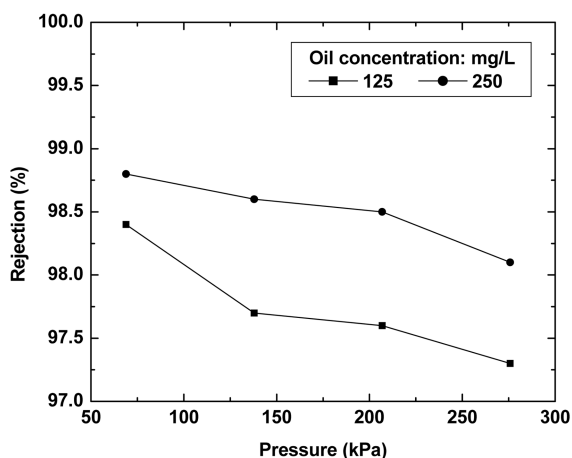


Fig.11 Variation of oil rejection at the end of 60 minutes of operation for feed oil concentration of 125 and 250 mg/L at different trans-membrane pressure drop

permeate flux reduces with increasing oil concentration. This was because of the fact that with an increase in feed concentration, adsorptive resistances as well as concentration polarization resistances increased and hence permeate flux decreased.

Fig. 11 illustrates the percent rejection of crude oil after 60 minutes of experimental run with varying trans-membrane pressure drops for feed oil concentration of 125 and 250 mg/L. From the figure, it can be observed that the percent oil rejection decreases marginally with increasing ΔP as well as oil concentration. For example, percent oil rejection decreases from 98.4 to 97.3% when pressure increases from 68.95 to 275.79 kPa for the initial oil concentration of 125 mg/L. This was due to the fact that higher pressures facilitate the enhancement of wetting and coalescence of oil droplets, thereby facilitating some oil droplets to pass through the membrane pores and reach the permeate stream. It may also be observed from the figure that percent oil rejection increases from 97.3 to 98.1% when initial oil concentration increases from 125 to 250 mg/L at 275.79 kPa. An increase in oil rejection efficiency with an increase in feed oil concentration was due to the higher droplet size of the emulsions. The oil rejection efficiency of the membrane was observed to increase marginally (less than 1%) with time. This was possibly due to the reduction in the membrane pore diameters that was accomplished by the adsorption of oil droplets in the membrane porous structure.

4. Cost of the membrane

Industrially competitive aspect of membrane technology lies in its cost. Table 2 summarizes the retail and bulk prices of various inorganic precursors that were used for the fabrication of the membranes. While the retail prices of the materials includes raw-material and shipment costs and not fabrication costs, the bulk prices only indicate the cost of the raw-materials and ignores shipment and fabrication costs. Based on the inorganic precursor formulation, the overall cost of the membranes using bulk and retail cost indices have also been presented in the table. While the retail prices of the precursors have been obtained from the catalog of companies summarized in section 2.1, the bulk prices have been obtained from various sources (ICIS 2009, China Glass Network

2009, U.S. Geological Survey 2006, Sichuan 2009). The cost of the membranes has been estimated to be 220 \$/m² and 1.53 \$/m² for retail and bulk prices of raw materials respectively. Both retail and bulk cost of the membrane cost based on the costs of the raw-materials is anticipated to be useful for providing small scale (such as research and pilot scale utilization of inorganic membranes) and large scale (industrial processing) applications of the fabricated membranes. Including shipment, fabrication and other costs, the average cost of inorganic membranes using large scale production methods may vary between 150 to 300 \$/m² (assuming 100-200 times the cost of the membrane based on bulk prices of the raw-materials). Contemporary elemental costs of various polymeric membranes and α -alumina ceramic symmetric membrane varies from 50 to 200 \$/m² and 2000 to 4000 \$/m², respectively (Tennison 2000). Therefore, it can be inferred from the cost analysis that the inorganic membrane based on kaolin would be closer to the cost of the polymeric membranes deployed for industrial configurations. However, the reported value of the membrane cost is conceptual in nature and may vary significantly depending on the fouling characteristics, membrane durability and life cycle of the ceramic membrane in process applications.

5. Conclusions

An inexpensive ceramic precursor formulation was identified utilizing locally available low cost inorganic raw materials such as kaolin, quartz, feldspar, sodium carbonate, boric acid and sodium metasilicate that can yield a submicron range ceramic membrane. Thermal, structural and morphological studies of the prepared membranes were carried out to evaluate the general characteristics of the fabricated ceramic membrane. Both liquid and gas permeation experiments were performed to evaluate general transport characteristics of the prepared membranes. The average pore size of the prepared ceramic membranes varied from 0.185 to 0.332 μm with total porosity of 34.4 to 19.5% when the sintering temperature varied from 800 to 950°C. Based on the retail and bulk prices of raw materials, the cost of membranes were evaluated to be 220 and 1.53 \$/m². Henceforth, the bulk cost of the fabricated membranes including materials, fabrication and shipment costs is suggested to be about 150 to 300 \$/m², a value comparable to that of the polymeric membranes. The membrane prepared at 950°C sintering temperature provided 98.8% oil rejection and 5.36×10^{-6} m³/m².s permeate flux after 60 minutes of experimental run at 68.95 kPa trans-membrane pressure and 250 mg/L oil concentration. Henceforth, the newly prepared ceramic membrane is suggested for application in chemical and biochemical processes using MF/UF techniques.

References

- Balek, V. and Murat, M. (1996), "The emanation thermal analysis of kaolinite clay minerals", *Thermochim. Acta.*, **282-283**, 385-397.
- Belouatek, A., Benderdouche, N., Addou, A., Ouagued, A. and Bettahar, N. (2005), "Preparation of inorganic supports for liquid waste treatment", *Micropor. Mesopor. Mat.*, **85**, 163-168.
- Bouzerara, F., Harabi, A., Achour, S. and Larbot, A. (2006), "Porous ceramic supports for membranes prepared from kaolin and dolomite mixtures", *J. Eur. Ceram. Soc.*, **26**, 1663-1671.
- Chakrabarty, B., Ghoshal, A.K. and Purkait, M.K. (2008a), "SEM Analysis and Gas Permeability Test to Characterize Polysulfone Membrane Prepared with Polyethylene Glycol as Additive", *J. Colloid Interf. Sci.*, **320**, 245-253.

- Chakrabarty, B., Ghoshal, A.K. and Purkait, M.K. (2008b), "Ultrafiltration of stable oil-in-water emulsion by polysulfone membrane", *J. Membrane Sci.*, **325**, 427-437.
- Chemical Industry news intelligence (2009), <http://www.icis.com>.
- Chen, G., Xing, H.Q.W. and Xu, N. (2008), "Direct preparation of macroporous mullite supports for membranes by in situ reaction sintering", *J. Membrane Sci.*, **318**, 38-44.
- China Glass Network (2009), <http://www.glassinchina.com>.
- Das, R. and Dutta, B.K. (1999), "Permeation and Separation Characteristics of Supported Alumina and Titania Membranes", *Sep. Sci. Technol.*, **34**, 609-625.
- DeFriend, K.A., Wiesner, M.R. and Barron, A.R. (2003), "Alumina and aluminate ultra-filtration membranes derived from alumina nanoparticles", *J. Membrane Sci.*, **224**, 11-28.
- Falamaki, C., Shafiee, A.M. and Aghaie, A. (2004), "Initial sintering stage pore growth mechanism applied to the manufacture of ceramic membrane supports", *J. Eur. Ceram. Soc.*, **24**, 2285-2292.
- Gestel, T.V., Vandecasteele, C., Buekenhoudt, A., Dotremont, C., Luyten, J., Leysen, R., Bruggen, B.V. and Maesc, G. (2002), "Alumina and titania multilayer membranes for nanofiltration: preparation, characterization and chemical stability", *J. Membrane Sci.*, **207**, 73-89.
- JCPDS (Joint Committee for Powder Diffraction Studies) (1997), *Powder Diffraction File of Inorganic Phases*, International Center for Diffraction Data, Swarthmore, PA, USA.
- Jedidi, I., Khemakhem, S., Larbot, A. and Amar, R.B. (2009), "Elaboration and characterization of fly ash based mineral supports for microfiltration and ultrafiltration membranes", *Ceram. Int.*, **35**, 2747-2753.
- Khemakhem, S., Larbot, A. and Ben Amar, R. (2009), "New ceramic microfiltration membranes from Tunisian natural materials: Application for the cuttlefish effluents treatment", *Ceram. Int.*, **35**, 55-61.
- Masmoudia, S., Larbot, A., Feki, H.E. and Amara, R.B. (2007), "Elaboration and characterisation of apatite based mineral supports for microfiltration and ultrafiltration membranes", *Ceram. Int.*, **33**, 337-344.
- Mulder, M. (1991), *Basic Principles of Membrane Technology*, Kluwer Academic Publishers, Dordrecht.
- Nandi, B.K., Uppaluri, R. and Purkait, M.K. (2008), "Preparation and characterization of low cost ceramic membranes for microfiltration applications", *Appl. Clay Sci.*, **42**, 102-110.
- Nandi, B.K., Uppaluri, R. and Purkait, M.K. (2009), "Effects of dip coating parameters on the morphology and transport properties of cellulose acetate-ceramic composite membranes", *J. Membrane Sci.*, **330**, 246-258.
- Potdar, A., Sukla, A. and Kumar, A. (2002), "Effect of gas phase modification of analcime zeolite composite membrane on separation of surfactant by ultra-filtration", *J. Membrane Sci.*, **210**, 209-225.
- Saffaj, N., Persin, M., Younsi, S.A., Albizane, A., Cretin, M. and Larbot, A. (2006), "Elaboration and characterization of micro-filtration and ultra-filtration membranes deposited on raw support prepared from natural Moroccan clay: Application to filtration of solution containing dyes and salts", *Appl. Clay Sci.*, **31**, 110-119.
- Saffaj, N., Younsi, S.A., Albizane, A., Messouadi, A., Bouhria, M., Persin, M., Cretin, M. and Larbot, A. (2004), "Preparation and characterization of ultra-filtration membranes for toxic removal from wastewater", *Desalination*, **168**, 259-263.
- Sichuan Yinfeng Chemical Co., Ltd. (2009), http://www.scyfchem.com/product4_e.htm.
- Tennison, S. (2000), "Current hurdles in the commercial development of inorganic membrane reactors", *Membrane Tech.*, **2000**(128), 4-9.
- U.S. Geological Survey (2006), *Kyanite and Related Materials Minerals Handbook*, 41.3.
- Wang, M.C., Wu, N.C. and Hon, M.H. (1994), "Preparation of nepheline glass-ceramics dental porcelain", *Mater. Chem. Phys.*, **37**, 370-375.
- Wang, Y.H., Tian, T.F., Liu, X.Q. and Meng, G.Y. (2006), "Titania membrane preparation with chemical stability for very harsh environments applications", *J. Membrane Sci.*, **280**, 261-269.
- Workneh, S. and Shukla, A. (2008), "Synthesis of sodalite octahydrate zeolite-clay composite membrane and its use in separation of SDS", *J. Membrane Sci.*, **309**, 189-195.
- Yoshino, Y., Suzuki, T., Nair, B.N., Taguchi, H. and Itoh, N. (2005), "Development of tubular substrates, silica based membranes and membrane modules for hydrogen separation at high temperature", *J. Membrane Sci.*, **267**, 8-17.